Computational Approach to Analyzing 3D Strain Distribution in Opaque Materials via Micro Computer Tomography

† Lingtao Mao[1], Haizhou Liu[1], and *Fu-pen Chiang[2]

[1] State Key Laboratory of Coal Resources and Safe Mining, China University of Mining & Technology, Beijing 100083, China

[2] Dept. of Mechanical Engineering, Stony Brook University, Stony Brook, NY 11794-2300, USA

* Presenting author: mlt@cumtb.edu.cn

† Corresponding author: mlt@cumtb.edu.cn

Abstract

In this paper we introduce a newly developed 3D stress/strain analysis technique, called digital volumetric speckle photography (DVSP), that has the capability of probing internal strain distribution inside opaque solids under load. We take advantage of X-ray computed tomography's ability to record 3D volumetric image of solids with internal markers such as impunities, voids, etc and treat them as 3D volumetric speckles. Under load these markers will move accordingly. We track their displacements via a two-stage 3D FFT process which is an extension of the 2D process used in 2D digital speckle photography technique developed in 1993 by F.P. Chiang and his coworkers. We have successfully applied DVSP to strain analysis of rocks, concrete, and composites. The resolution of the technique is a function of the hardware used. It varies from macro scale with a medical X-ray CT, to micro scale with an industrial X-ray CT, and to nano-scale with a synchrotron radiation CT.

Keywords: 3D strain analysis, digital volumetric speckle photography, computed tomography, FFT.

Introduction

Digital Speckle Photography (DSP) technique evolves from the speckle photography technique originally proposed by J Burch in 1968 years before the invention of lasers. Over the years, it has evolved into techniques such as laser speckle photography, electron speckle photography, white light speckle photography, and one-beam laser speckle interferometry. Up until the advent and ubiquitous usage of digital camera, the process of generating useful information from a specklegram is always done by using a laser beam. In the pointwise approach, a narrow laser beam is directed at a point of a double exposed specklegram. The resulting diffraction pattern consists of a circular halo modulated by an array of parallel fringes, which can be related to the magnitude and direction of the displacement vector experienced by the cluster of speckles within the diameter of the laser beam. For the full field approach, an optical spatial filtering process is employed to display the displacement contours resolved along a particular direction with a sensitivity corresponding to the particular spatial frequency. In the early 1990s the process was digitalized by Chiang and his coworkers[1]. Only the surface deformation of a plane object can be obtained using this 2D-DSP technique.

With the aid of advanced imaging devices, such as high-resolution X-ray computer tomography (Micro CT), micro magnetic resonance imaging (micro-MRI) or laser scanning confocal microscope (LSCM), high-spatial-resolution volumetric images of opaque or semi-transparent materials can be acquired. Combined these advanced imaging devices with 2D Digital Image Correlation (DIC), a novel and useful technique for the quantification of 3D internal deformation, a new technique called DVC(Digital Volume Correlation) has emerged. The DVC method is a 3D extension of 2D-DIC, first proposed by Bay et al for strain analysis in bone [2]. By extending the 2D-DSP, Chiang and Mao recently developed a new 3D strain analysis technique called Digital Volumetric Speckle Photography (DVSP) [3], which offers a higher computational efficiency than DVC by using the FFT (fast Fourier transform) algorithm. In this paper we present the theory of DVSP and its application to 3D strain analysis of rock, concrete and woven composite.

Theory of Digital Volumetric Speckle Photography(DVSP)

Digital volume images of a 3D solid before and after deformation are reconstructed with advanced imaging techniques using a CT or a MRI (either micro or macro). These two volume images are defined as reference volume image and deformed volume image, respectively. Both of them are divided into volumetric subsets with voxel arrays of $32\times32\times32$ voxels, for example, and 'compared'. The principle is schematically shown in Fig. 1. Based on the theory of 2D digital speckle photography[1, 4], the DVSP principle is as follows[5]:

Let $h_1(x,y,z)$ and $h_2(x,y,z)$ be the gray distribution functions of a pair of generic volumetric speckle subsets, before and after deformation, respectively, and that

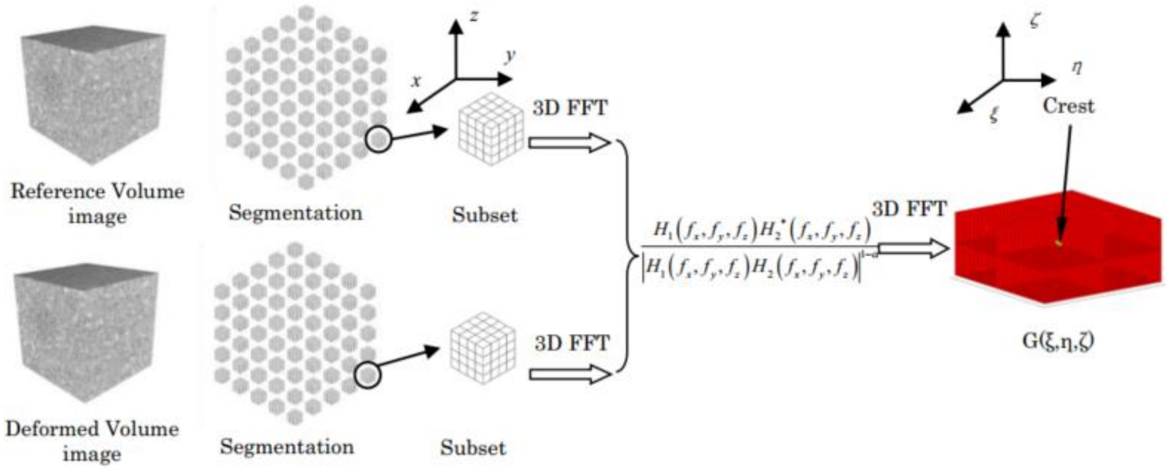

Fig.1 Schematics demonstrating the processing algorithm of DVSP

$$h_1(x,y,z) = h(x,y,z)$$

$$h_2(x,y,z) = h[x-u(x,y,z), y-v(x,y,z), z-w(x,y,z)] \tag{1}$$

where *u*, *v* and *w* are the displacement components experienced by the speckles along the *x*, *y*, and *z* directions, respectively. A first-step 3D FFT (Fast Fourier Transform) is applied to both h_1 and h_2 yielding

$$\begin{aligned} H_1(f_x,f_y,f_z) &= \Im\{h_1(x,y,z)\} = |H(f_x,f_y,f_z)|\exp[j\phi(f_x,f_y,f_z)] \\ H_2(f_x,f_y,f_z) &= \Im\{h_2(x,y,z)\} = |H(f_x,f_y,f_z)|\exp\{j[\phi(f_x,f_y,f_z) - 2\pi(uf_x+vf_y+wf_z)]\} \end{aligned} \tag{2}$$

where $H_1(f_x,f_y,f_z)$ is the Fourier transform of $h_1(x,y,z)$, $H_2(f_x,f_y,f_z)$ is the Fourier transform of $h_2(x,y,z)$, and $\Im$ stands for Fourier Transform. $|H(f_x,f_y,f_z)|$ and $\phi(f_x,f_y,f_z)$ are spectral amplitude and phase fields, respectively.

Then, a numerical interference between the two 3D speckle patterns is performed at the spectral domain, i.e.

$$F\left(f_x, f_y, f_z\right) = \frac{H_1\left(f_x, f_y, f_z\right) H_2^*\left(f_x, f_y, f_z\right)}{\left|H_1\left(f_x, f_y, f_z\right) H_2\left(f_x, f_y, f_z\right)\right|^{1-\alpha}} \tag{3}$$

where * stands for the complex conjugate, and α is an appropriate constant $(0 \leq \alpha \leq 1)$.

When $\alpha = 0$, Eq.(3) can be expressed as

$$F\left(f_x, f_y, f_z\right) = H_1\left(f_x, f_y, f_z\right) \frac{\exp\left\{-j\left[\phi\left(f_x, f_y, f_z\right) - 2\pi\left(uf_x + vf_y + wf_z\right)\right]\right\}}{\left|H\left(f_x, f_y, f_z\right)\right|} \tag{4}$$

where $\frac{\exp\left\{-j\left[\phi\left(f_x, f_y, f_z\right) - 2\pi\left(uf_x + vf_y + wf_z\right)\right]\right\}}{\left|H\left(f_x, f_y, f_z\right)\right|}$ is essentially an inverse filter (IF).

When $\alpha = 0.5$, Eq.(3) can be expressed as

$$F\left(f_x, f_y, f_z\right) = H_1\left(f_x, f_y, f_z\right) \exp\left\{-j\left[\phi\left(f_x, f_y, f_z\right) - 2\pi\left(uf_x + vf_y + wf_z\right)\right]\right\} \tag{5}$$

where $\exp\left\{-j\left[\phi\left(f_x, f_y, f_z\right) - 2\pi\left(uf_x + vf_y + wf_z\right)\right]\right\}$ is a so-called phase-only filter (POF).

When $\alpha = 1$, Eq.(3) can be expressed as

$$F\left(f_x, f_y, f_z\right) = H_1\left(f_x, f_y, f_z\right) H_2^*\left(f_x, f_y, f_z\right) \tag{6}$$

where $H_2^*\left(f_x, f_y, f_z\right)$ can be viewed as a classical matched filter(CMF). When a correlation filter is chosen, Peak sharpness and noise tolerance are the criteria to be considered. In the 2D digital speckle photography technique [1,4], α is 0.5, and the algorithm is essentially a POF. In Ref. [6] the influence of CMF, POF and IF filters on the accuracy of 2D electronic speckle photography were analyzed and the results indicated that IF is extremely sensitive to noise, thus cannot be used as a reliable filter. There is no significant difference between CMF and POF filters. But while the POF filter provides somewhat more accurate estimates of the peak position, the reliability of the CMF filter is better. In Fig.2 , normalized impulse function distribution are shown. It is noted that the peak impulse with POF is sharper.

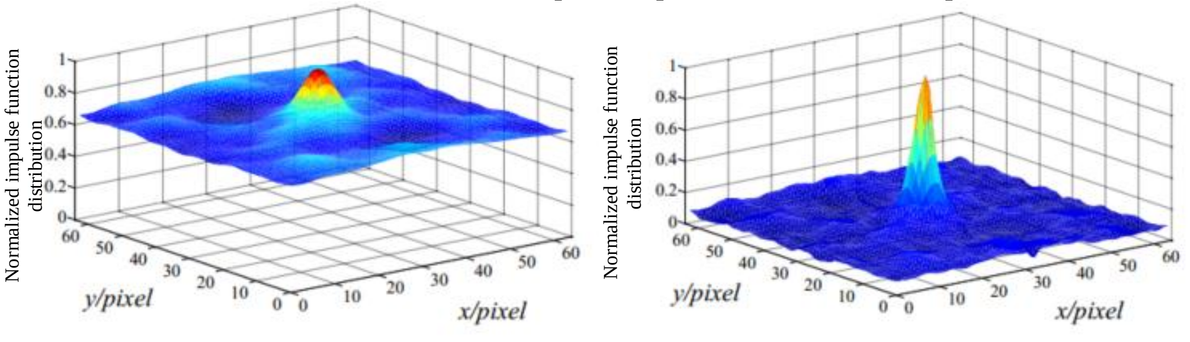

(a) (b)

Fig.2 Normalized impulse function distribution with different filter (a) CMF filter; (b) POF filter

In this paper, $\alpha = 0.5$ is adopted. As a result Eq.(3) can then be written as

$$F(f_x, f_y, f_z) = \frac{H_1(f_x, f_y, f_z) H_2^*(f_x, f_y, f_z)}{\sqrt{|H_1(f_x, f_y, f_z) H_2(f_x, f_y, f_z)|}} = |H_1(f_x, f_y, f_z)| \exp\{j[\phi_1(f_x, f_y, f_z) - \phi_2(f_x, f_y, f_z)]\} \tag{7}$$

where $\phi_1(f_x, f_y, f_z)$ and $\phi_2(f_x, f_y, f_z)$, are the phases of $H_1(f_x, f_y, f_z)$ and $H_2(f_x, f_y, f_z)$, respectively. It is seen that

$$\phi_1(f_x, f_y, f_z) - \phi_2(f_x, f_y, f_z) = 2\pi(uf_x + vf_y + wf_z) \tag{8}$$

Finally, a function is obtained by performing another 3D FFT resulting

$$G(\xi, \eta, \zeta) = \Im\{F(f_x, f_y, f_z)\} = \bar{G}(\xi - u, \eta - v, \zeta - w) \tag{9}$$

which is an expanded impulse function located at (*u*, *v*, *w*). This process is carried out for every corresponding pair of the subsets. By detecting the crest of all these impulse functions, an array of displacement vectors at each and every subset is obtained, from which strain tensors can be calculated using an appropriate strain-displacement relation.

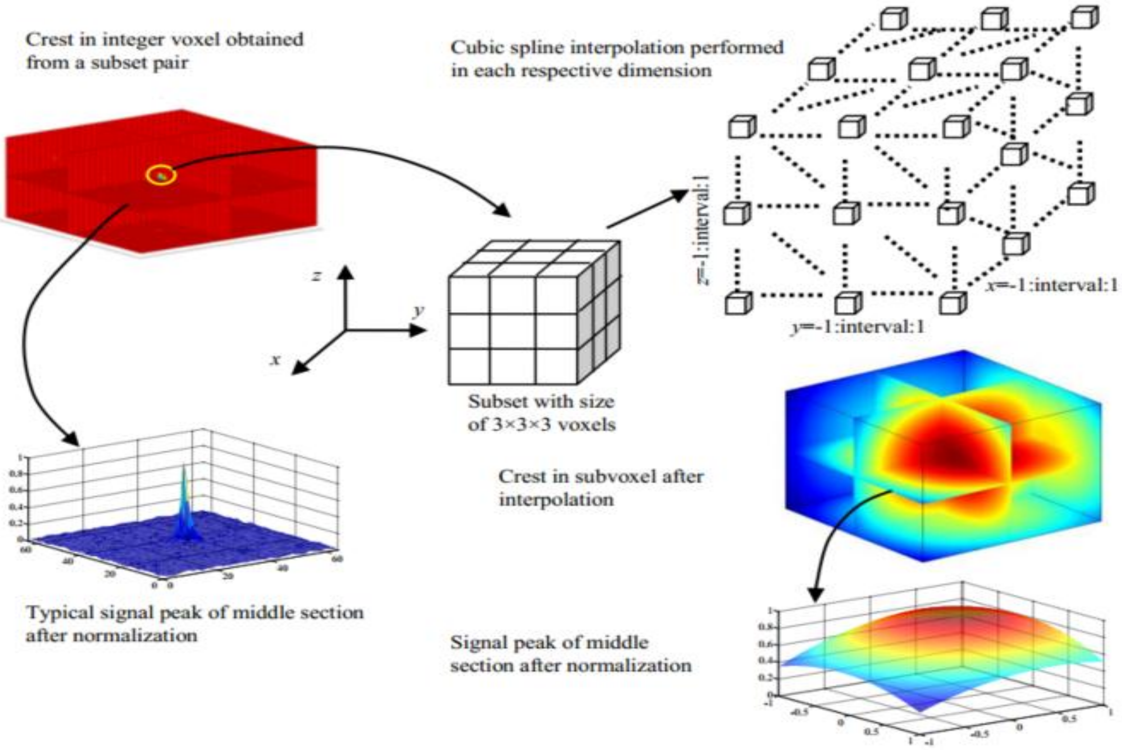

Fig.3 Schematics showing the interpolation procedure

In the above analysis the deformation of the subset itself is neglected. Because of the discrete nature of digital volume images, the displacement vectors evaluated from equation (9) are integral multiples of one voxel. In order to obtain more accurate and sensitive characterization, a sub-voxel investigation of the crest position is needed. To achieve this, we select a cubic subset with $3\times3\times3$ voxels surrounding an integral voxel of the crest and a cubic spline interpolation is employed to obtain the interpolated values among the integral voxels in each respective dimension. After interpolation, the cubic subset is enlarged and a new three dimensional array is generated with size depending on the interpolation interval. The smaller the interval and the bigger the array size give rise to higher interpolation accuracy. The price to pay, however, is the need for more computational time and more memory space. In practical applications there would be a tradeoff between the two competing needs. By detecting the positions of peak values of the new array, displacements of subvoxel accuracy can be obtained. The interpolation procedure is illustrated schematically in Fig.3.

Strain estimation

The internal strain tensor ε can be derived from the displacement fields. Due to the influence of unavoidable noise contained in the CT images, the displacements determined above contains discontinuities or noise that are not a feature of the material but a consequence of the discrete nature of the analysis performed. The errors in the local displacements may be amplified during the strain computation process. By using PLS (Point Least-Squares) approach, the errors can be largely reduced during the process of local fitting, and the strains estimated will be more accurate [7].

The element of PLS approach is shown as followings. To compute the local strains of each considered point, a regular cubic box with size of $(2N+1)\times(2N+1)\times(2N+1)$ discrete points surrounding the point is selected. If the strain calculation window is small enough, the displacements in each direction can be reasonably assumed to be linearly distributed, and therefore can be mathematically expressed as

$$\begin{aligned} u(x,y,\mathrm{z}) &= a_0 + a_1 x + a_2 y + a_3 z \\ v(x,y,\mathrm{z}) &= b_0 + b_1 x + b_2 y + b_3 z \\ w(x,y,\mathrm{z}) &= c_0 + c_1 x + c_2 y + c_3 z \end{aligned} \tag{10}$$

where x, y, z = $[-N,N]$are the local coordinates within the strain calculation box, $u(x, y, z)$, $v(x, y, z)$ and $w(x, y, z)$ are the displacements directly obtained by DVSP method, and $a_{i=0,1,2,3}$, $b_{i=0,1,2,3}$ and $c_{i=0,1,2,3}$ are the unknown polynomial coefficients to be determined. With the Least-squares or Multiple Regression Analysis, the unknown coefficients can be estimated. Then, the six Cauchy strain components ε_x, ε_y, ε_z, ε_{xy},ε_{xz} and ε_{yz} at the interrogated point can thus be calculated as

$$\begin{aligned} &\varepsilon_x = \frac{\partial u}{\partial x} = a_1 \quad \varepsilon_{xy} = \frac{1}{2}\left(\frac{\partial v}{\partial x} + \frac{\partial u}{\partial y}\right) = \frac{1}{2}(b_1 + a_2) \\ &\varepsilon_y = \frac{\partial v}{\partial y} = b_2 \quad \varepsilon_{yz} = \frac{1}{2}\left(\frac{\partial w}{\partial y} + \frac{\partial v}{\partial z}\right) = \frac{1}{2}(c_2 + b_3) \\ &\varepsilon_z = \frac{\partial w}{\partial z} = c_3 \quad \varepsilon_{xz} = \frac{1}{2}\left(\frac{\partial u}{\partial z} + \frac{\partial w}{\partial x}\right) = \frac{1}{2}(a_3 + c_1) \end{aligned} \tag{11}$$

With these Cauchy strain components, the principal strains can be calculated, and then the deviatotic strain ε_s and the volumetric strain ε_v are written as

$$\varepsilon_s = \frac{\sqrt{2}}{3}\sqrt{(\varepsilon_1-\varepsilon_2)^2 + (\varepsilon_2-\varepsilon_3)^2 + (\varepsilon_3-\varepsilon_1)^2} \tag{12}$$

$$\varepsilon_v = \varepsilon_1 + \varepsilon_2 + \varepsilon_3 \tag{13}$$

where ε_1, ε_2 and ε_3 are the major, intermediate and minor principal strains, respectively.

X-ray Micro-CT

Over the years, medical CT scanners have been drastically improved in terms of image quality, imaging speed and deposited radiation dosage. But the spatial resolution remains limited to several hundreds of micrometres due to the dimension of the investigated object, i.e. a human patient. The micro-CT with high-resolution has emerged in the 1980s. Based on the type of X-ray generation, X-ray micro-CT can be divided into synchrotron-based and lab-based micro-CT (using X-ray tubes). Since synchrotron sources have a high X-ray flux, X-ray optics can be used to achieve very high spatial resolution up to tens of nanometers. Combined with different CT scanners, the resolution of DVSP varies from macro scale with a medical x-ray CT, to micro scale with an industrial x-ray CT, and to nano scale with a synchrotron radiation CT.

In this study, the main components of the industrial X-Ray computer tomography system are a microfocus X-ray source from YXLON (Feinfocus 225kV), an X-ray detector unit (1024×1024 pixels) from PerkinElme (XRD 0822AP 14), and a motorized rotation stage from Newport. The X-ray has a focus with size of 3 × 6 μm, a voltage range of 50-225kV, and the tube current ranging from 0 to 1440μA. A uniaxial compression setup has been designed and built to allow performing micro-tomography of a specimen under load (in situ).

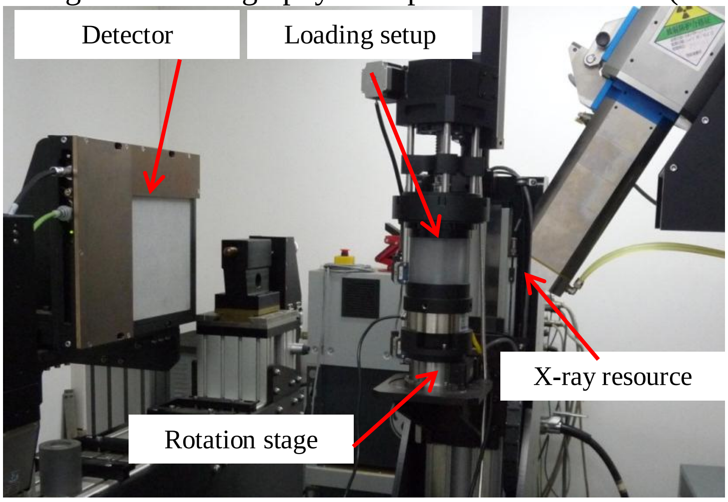

Fig.4 The Micro-CT system and the loading setup used to record the volumetric image of the specimen at each loading step

Applications of DVSP

Internal Strain Analysis of Red Sandstone with a Pre-existing Crack under Uniaxial Compression

A cuboid sample of red sandstone with a pre-existing crack under uniaxial compression was scanned in situ using the X-ray CT system. The sample has the size of 23 mm (L)× 10mm(W)× 40 mmc(H). A partial circular surface crack with an inclination of 45° with respect to the loading axis is carved into the specimen as shown in Fig5(a). The whole compression process was divided into 4 steps. The load-displacement history, reconstructed 3D images of Step 3 and Step 4, and a meridian slice of the specimen are shown in Fig.5 (a) , (b), (c), and (d), respectively. The volume image of step 1 was used as the reference image.

The subsequent deformed images were “compared” to the reference image via the DVSP method and resulted in displacement contours. The sectional image along section AA’ shown in Fig.5(d) is depicted in Fig.5(e), and the u, v, w displacement fields and ε_{yz} strain distributions are plotted in Fig.5 (f),(g), (h), and (i), respectively.

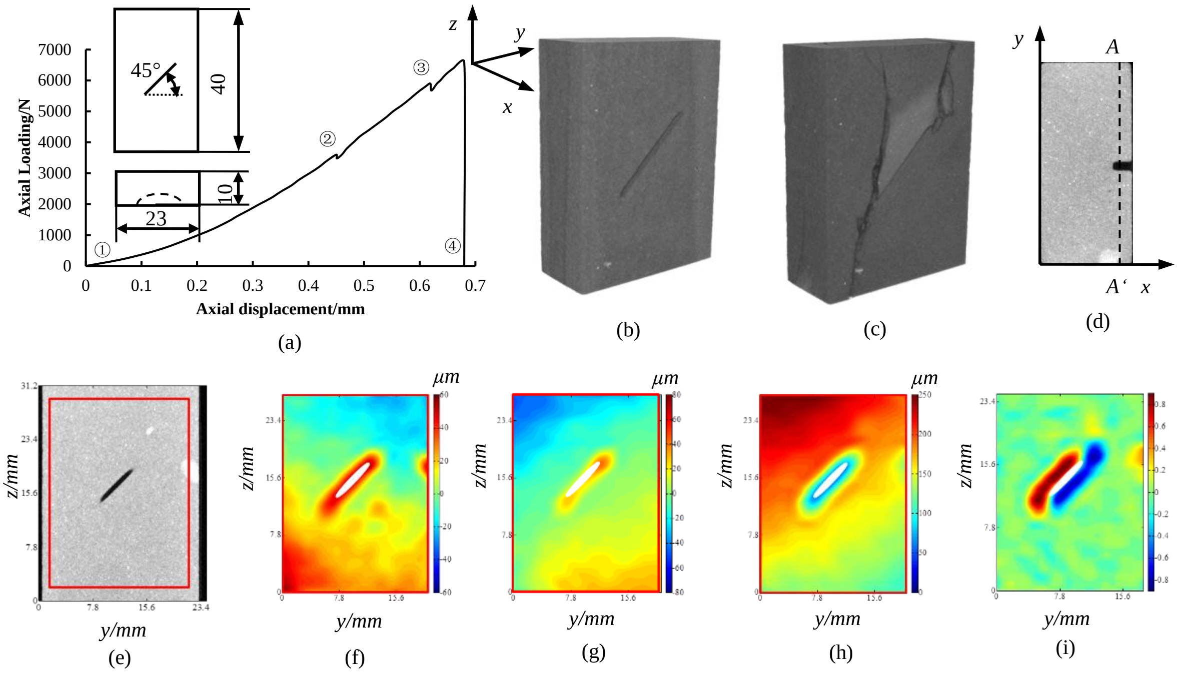

Fig.5 Application in red sandstone with pre-existing crack under Uniaxial Compression; (a) Load-displacement curve; (b) and (c) are reconstructed 3D images of Step 3 and Step 4; (d) Meridian slice; (e) Section along AA’; (f) u-field; (g) v-field; (h) w-field; (i) εyz strain

Internal Strain Analysis of Concrete under Uniaxial Compression

The concrete specimen is made from the subgrade of one highway. The size of the specimen is Φ25×48 mm. The compaction of the specimen was achieved by applying a compressive load in the axial (z) direction. The whole compression process was divided into 8 loading steps. In each step, the loading was kept constant while the specimen was scanned. By using DVSP we calculated the displacement and strain distributions in different sections of the specimen.

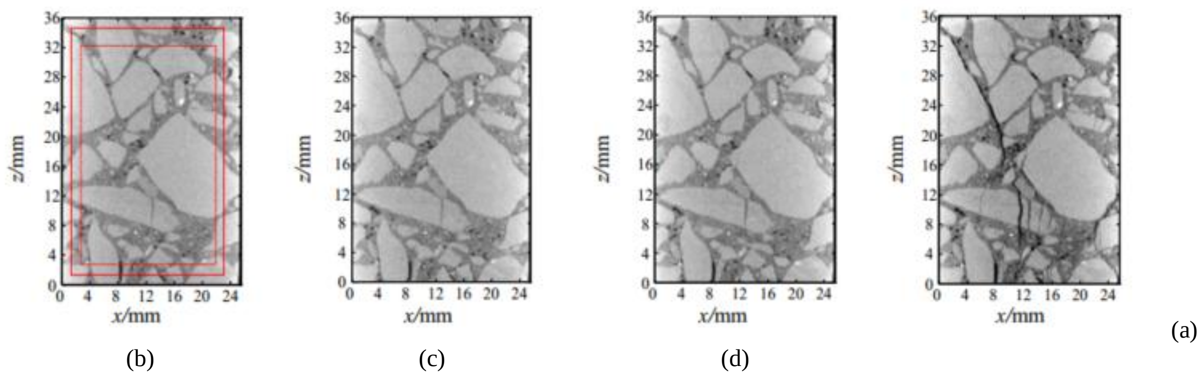

Fig.6.Reconstructed meridian sectional images under different loading; (a)5.3MPa ;(b)14.80MPa ; (c) 18.50MPa;(d)24.70MPa

Fig.6 shows the reconstructed meridian section images under different loading conditions. It is difficult to detect cracks from these gray images until the loading is at 24.70 MPa. Fig.7 shows the distributions of the major principal strain of the meridian section corresponding to the pictures shown in Fig.6. The light yellow mainly occurs at interface zones between aggregates and mortar which indicates the higher strain value appearing in these zones. The specimen tends to break at interface zones as demonstrated in Fig.6 (d).

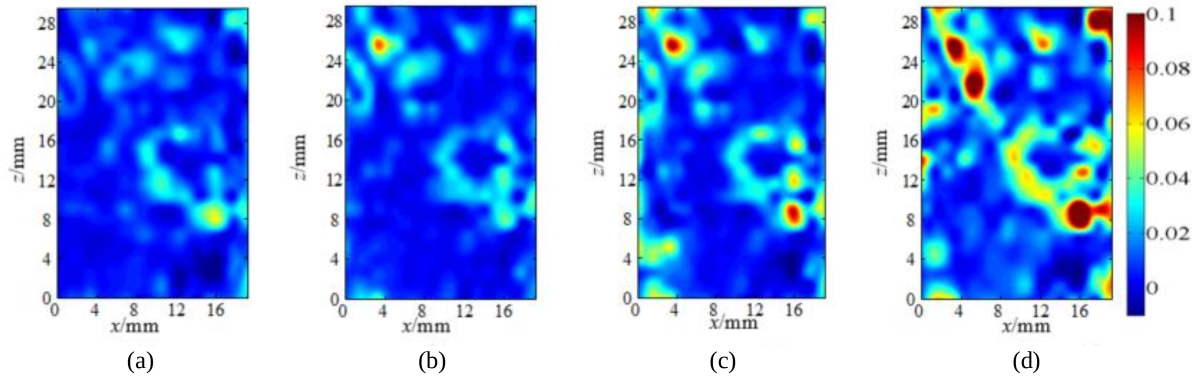

Fig. 7. Distribution contours of the first principal strain; (a)5.3MPa ;(b)14.80MPa ; (c) 18.50MPa;(d)24.70MPa

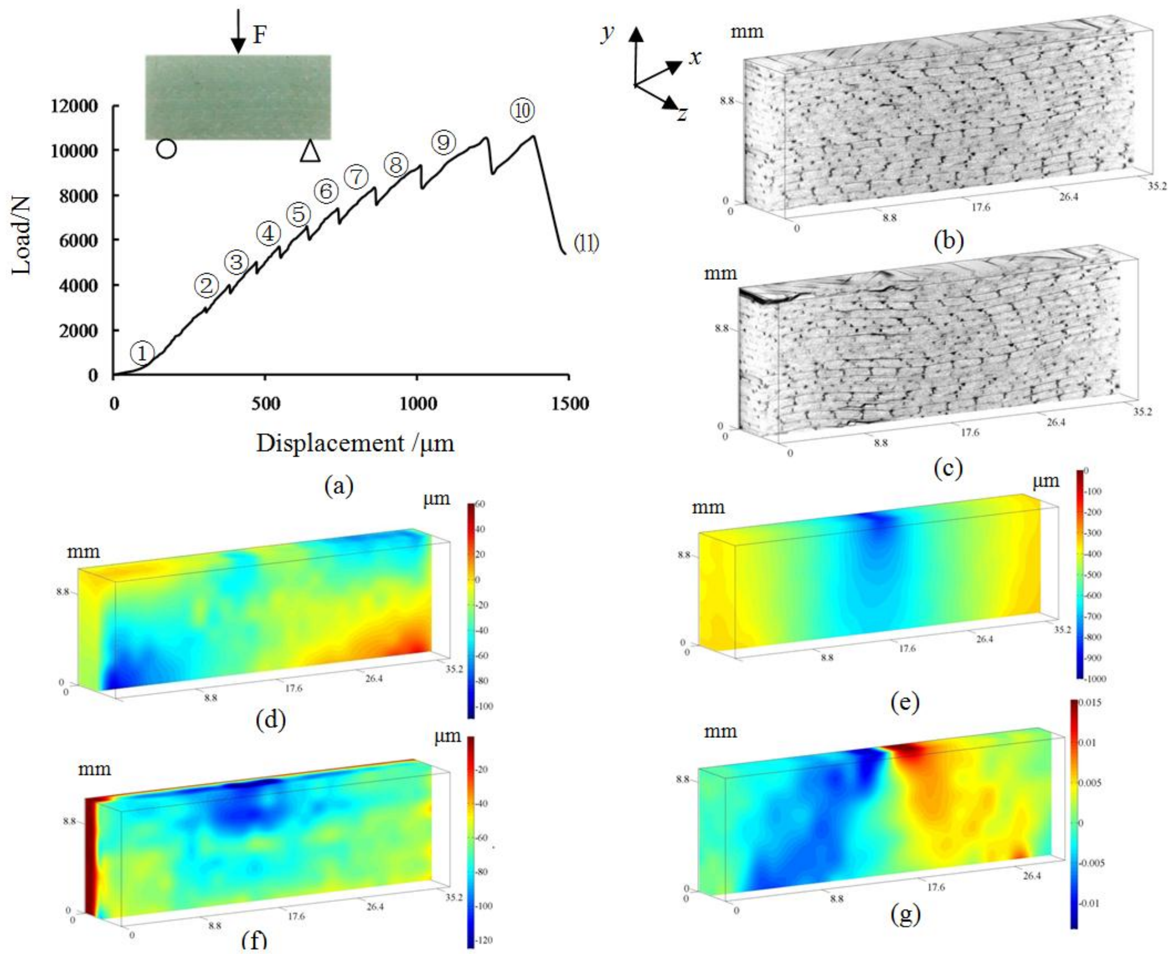

Fig. 8. Load-displacement curve , section images and deformation contours(a) Load-displacement curve (b) section image of Step 10; (c) Section image of Step 11; (d) u-field of section image of Step 10; (e) v-field of section image of Step 10; (f) w-field the section of Step 10, (g) ε_{xy} contours of the section;

Internal Strain Analysis of Composite under 3-point Bending

A tri-direction woven fabric composite beam with the size of 40mm(L)×19mm(H)×9mm(T) under 3-point bending was scanned in situ[8]. The matrix of the composite is epoxy resin, occupying 55% by volume. The filament diameter is 17μm. The experimental process is divided into 11 Step. The load-displacement curve, section images of Step 10 and Step 11 are shown in Fig 8(a), (b), and (c), respectively. The displacement and strain fields are presented in Fig.8 (d), (e), (f), and (g), respectively. As can be seen from the pictures that it is easy to detect the process of deformation localization.

Summary

We have demonstrated that the DVSP method can be effectively applied to analyzing internal strain distribution of red sandstone, concrete and composite, and we believe the DVSP technique has the potential of advancing the art of all 3D stress/strain analysis.

Acknowledgements

This work was financially supported by National Natural Science Foundation of China (51374211), State Key Research Development Program of China (2016YFC0600705), National Key Foundation for Exploring Scientific Instrument of China (2013YQ240803),and ONR Solid Mechanics Program grant N0014-14-1-0419 directed by Dr.Yapa Rajapakse.

References

[1] Chen D.J., Chiang F.P., Tan Y.S., et al. (1993) Digital speckle-displacement measurement using a complex spectrum method, App. Opt. 32, 1839-1849
[2] Bay B. K., Smith T. S., Fyhie D. P., et al, (1999) Digital volume correlation: Three-dimensional strain mapping using X-ray tomography, Experimental Mechanics 39, 217-226
[3] Chiang F.P. ,Mao L.T., (2015) Development of Interior Strain Measurement Techniques Using Random Speckle Patterns, Meccanica 50, 401–410
[4] F. P. Chiang, Super-resolution digital speckle photography for micro/nano measurements, Optics and lasers in Engineering, 47(2009):274-279
[5] Mao Lingtao, Fu-pen Chiang, 3D Strain Mapping in Rocks Using Digital Volumetric Speckle Photography Technique, Acta Mechanica，2016,227(11):3069-3085
[6] M. Sjodahl, Accuracy in electronic speckle photography, App. Opt., 36(13) (1997): 2875-2885
[7] B. Pan, D. F. Wu, Z. Y. Wang, Internal displacement and strain measurement using digital volume correlation : a least-squares framework, Measurement Science and Technology, 23(2012): 45002-45014
[8] Mao L.T., Chiang F.P. , (2015) Interior Strain Analysis of a Woven Composite Beam Using X-ray Computed Tomography and Digital Volumetric Speckle Photography, Composite Structures 134, 782-788